ACS Photonics

pubs.acs.org/journal/apchd5

Article

Visualizing the Transient Response of Local Potentials on Photoconductive Antennas Using Scanning Ultrafast Electron Microscopy

Yusuke Arashida,* Samuel Jeong,* Kouhei Kawasaki, Yuga Emoto, Godai Noyama, Masaki Hada, Yoshiya Kishibe, Hidemi Shigekawa, Keishi Akada, Shoji Yoshida, and Jun-ichi Fujita*

Cite This: *ACS Photonics* 2024, 11, 2171−2175

Read Online

ACCESS | Metrics & More | Article Recommendations | Supporting Information

ABSTRACT: Scanning electron microscopy (SEM) has been widely used to evaluate nanoscale images of materials and devices by measuring the current of secondary electrons (SEs). We developed scanning ultrafast electron microscopy by combining a commercially available SEM and a femtosecond laser to reveal the local dynamic properties of broadband electric devices during operation. We conducted pump−probe experiments and successfully visualized the distribution of electric potential on the electrodes of a photoconductive antenna during a transient response induced by optical excitation of photocarriers in the semiconductor substrate of the device. The temporal resolution was determined to be 43 ps based on the pulse duration of the primary electrons under the space charge effect. The observed waveform of the SE current exhibited several phenomena, including ultrafast carrier dynamics at the boundaries, carrier lifetime, and electric circuit response. The proposed technique is expected to provide a new method for visualizing the operation of high-frequency electronic devices.

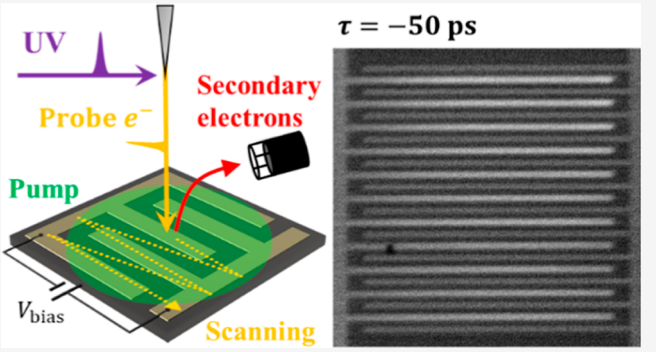

KEYWORDS: *scanning electron microscopy, femtosecond laser, time-resolved measurements, electric circuits, photoconductive antennas, transient responses*

INTRODUCTION

Rapid progress in electronic devices with high integration, high frequency, and low power consumption has accelerated recent information technology advances.[1,2] One method of achieving these devices involves reducing the size of device elements. However, it has become increasingly difficult to microscopically evaluate high-speed operations for electric measurements. Thus, obtaining a direct understanding of local electric potential, carrier diffusion, plasmon, etc., in high-frequency regions is important.[3−6]

Scanning electron microscopy (SEM) measures secondary electrons (SEs) to obtain microscopic pictures of materials with high spatial resolutions.[7,8] The amount of emitted SEs is dependent on the scattering cross-section of materials and the local electric potentials of the surfaces. SEM has been widely used to observe the structures of electronic devices,[4,9,10] particles,[11] metamaterials,[12−14] and microelectromechanical systems[9,15] with a spatial resolution of several nanometer and turnability of magnification. Recently, time-resolved measurements, known as scanning ultrafast electron microscopy (SUEM), have been performed using pulsed electrons photoemitted by femtosecond ultraviolet lasers.[16−24] The diffusion dynamics and lifetimes of the photoexcited carriers on semiconductors and photon junctions are discussed. This study demonstrated the observation of ultrafast snapshots of the local surface potentials of an operand photoconductive antenna. This technique is expected to provide new insights into the study of high-frequency electronic devices.

METHODS

The schematic of the setup is shown in Figure 1a. The fundamental light source was a Yb:KGW pulsed laser amplifier (Pharos, Light Conversion Inc.) with a center wavelength of 1030 nm (=1.2 eV), pulse duration of 190 fs, pulse energy of 100 μJ, and repetition frequency of 100 kHz. The fundamental beam was split into two beams with a power ratio of 1:9. The weaker beam was entered into a barium borate (BBO) crystal

Received: October 23, 2023
Revised: April 20, 2024
Accepted: April 22, 2024
Published: May 8, 2024

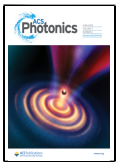

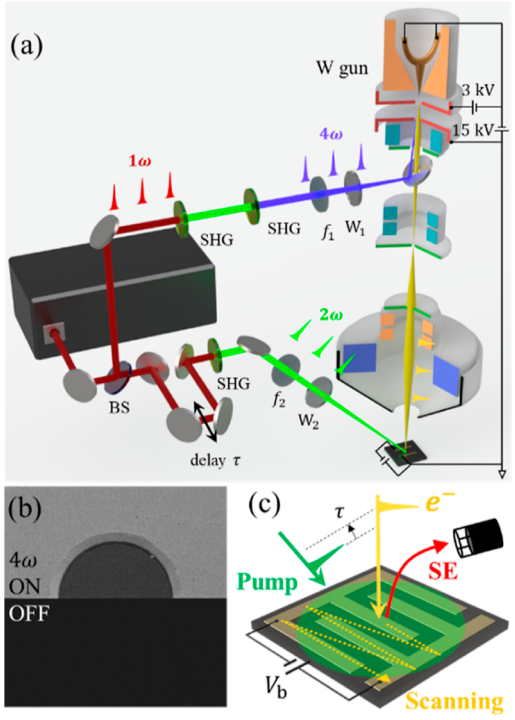

Figure 1. (a) Schematic of the SUEM. BS: beam splitter, SHG: second harmonic generation, $f_{1,2}$: convex lenses with the focal length of 300 and 750 mm, respectively, and $W_{1,2}$: optical windows of fused silica and BK7, respectively. (b) SE image of a holed aluminum plate with and without illuminating the 4ω beam to the tip of the gun (ON and OFF) while scanning the primary electrons slowly. (c) Scheme of pump−probe measurements on a photoconductive switch consists of Au electrodes and a GaAs substrate.

to generate second harmonic light (2ω) with a photon energy of 2.4 eV, which was used to excite photocarriers in a semiconducting sample. The other beam was converted to fourth harmonic light (4ω) with a photon energy of 4.8 eV using two BBO crystals. The 4ω was entered into the vacuum chamber of an SEM (JSM7200F, JEOL) and subsequently reflected via a hole-punched mirror (Figure S1) to enter the Shottky-emission electron gun made of tungsten. The photoemitted electron pulses propagated in a direction opposite that of the light. The electrons entered the samples after passing through the mirror hole, an objective aperture, and scanning coils. The extraction and acceleration voltages were 3 and 15 kV, respectively. We measured the number of SEs using an SE detector consisting of a collecting electrode at 300 V, a scintillator, and a photomultiplier tube. The filament current was 0 A; thus, no electrons were emitted from the gun without using the 4ω, as shown in Figure 1b. In the proposed SUEM system, each electron pulse consists of 6323 ± 679 electrons. The space charge effect expanded the electron pulse during the 65 cm flight from the electron gun to the sample surface and spread the energy width of electrons which might be the same order of 19 ± 10 eV (see Supporting Information S2). The spatial resolution was limited to approximately 200 nm by the spread of the electron pulse (Figure S3). As shown in Figure 1c, the pump-induced change of the state of the sample modulated the SE current, which was dependent on the delay time τ between the pump and electron pulses. To obtain an instantaneous SE image, we scanned the positions of the primary electrons with fixed delay times. To obtain the temporal waveform of the SE current at fixed positions, we fixed the positions of the primary electrons, scanned the delay time, and measured the SE current using a lock-in amplifier with a mechanical chopper on the pump beam.

We used interdigital array electrodes (IDAs) as the samples. IDAs have been widely used in surface acoustic wave filters,[25−27] generation and detection terahertz waves,[28,29] ultrafast photoconductive switches,[30] and RF resonators.[31,32] We patterned Au electrodes with a thickness of 200 nm on an undoped GaAs substrate (E_g ∼ 1.45 eV) using photolithography and Au spattering (Figure S4). As shown in Figure 2c, a bias voltage (V_b) was applied between the anode

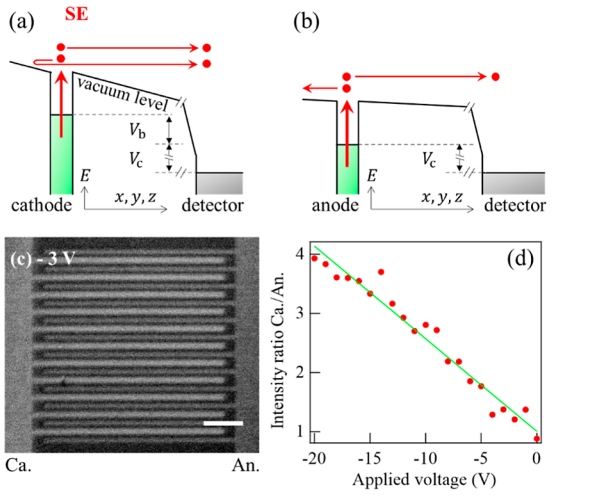

Figure 2. Schematic of the flow of SEs from the (a) cathodes and (b) anodes to the SE detector with the collection voltage V_c = 300 V. (c) SE image of the device with V_b = −3 V. Scale bar: 100 μm. (d) Ratio of the SE intensity of the cathodes and anodes (red) as a function of the voltage extracted by the integrated intensity of all electrodes for cathodes and anodes. The green line is the linearly fitted result.

and the cathode of the IDA, which acted as a capacitor. The anode was connected to the ground (GND). By considering the three-dimensional motion of SE, a larger number of electrons from the cathodes reach the detector than from the anodes to the detector, as shown in Figure 2a,b. A SEM image with V_b = −3 V is shown in Figure 2c. Larger SE currents were observed at the cathode than that at the anode. Note that the GaAs substrate exhibited a smaller SE current than both the electrodes because of the different work function or surface contamination owing to the effect of photolithography.

To calibrate the SE intensity to voltage, we measured the intensity ratio of the cathode to that of the anode as a function of V_b, as shown in Figure 2d. The intensity of the two electrodes was the same at V_b = 0 V and monotonically increased with increasing V_b. The linear fitting (green line) shows the intensity ratio $B(V_b) = -0.17\ V_b + 1.0$. We can convert the intensity ratio to voltage in the time-resolved measurements, as discussed below.

RESULTS AND DISCUSSION

We demonstrate photoconductive switching on a device wherein a biased capacitor was discharged by photocarriers in the GaAs substrates excited by femtosecond pump pulses. Instantaneous SEM images were observed by changing the delay time, τ between the pump and probe. At V_b = −20 V, the fully charged device was visualized at the delay time of −50 ps

https://doi.org/10.1021/acsphotonics.3c01532
ACS Photonics 2024, 11, 2171−2175

(the electron probe was incident to the sample before the pump), as shown in Figure 3a. A large difference was observed

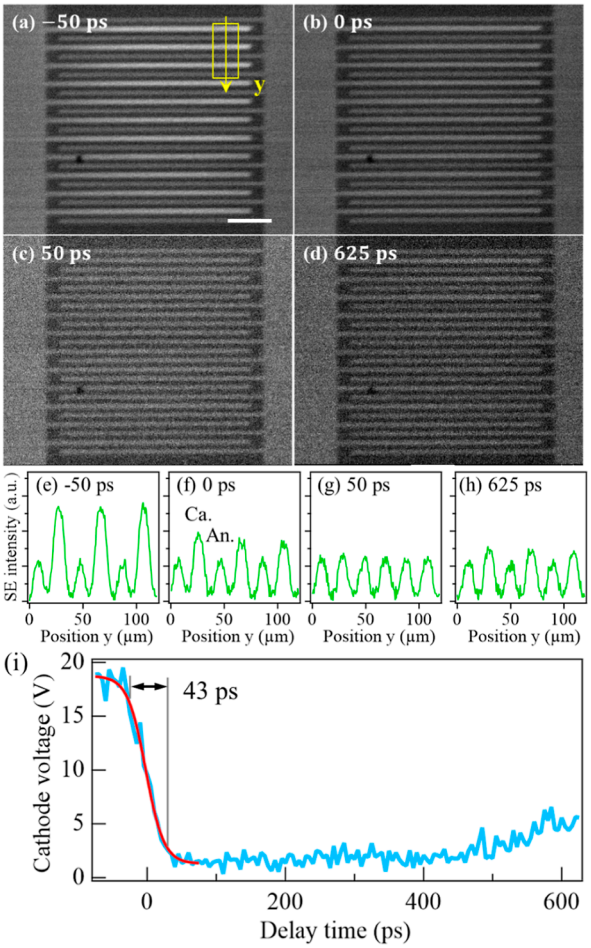

Figure 3. (a−d) Time-resolved SEM image with different delay times under V_b = −20 V. Scale bar 100 μm. (e−h) Line profile of SE intensity for different delays of (a−d), respectively. The integrated region is shown in Figure 3a. (i) Transient change of the cathode potential (blue) as a function of delay time. Red curve is the result of the fitting (see the text).

in the intensities of the cathodes and anodes, similar to the static image in Figure 2c. Furthermore, at τ = 0 ps, as shown in Figure 3b, the intensity ratio of the cathodes and anodes reduced owing to being discharged by the photoexcited carriers, where the carriers around the metal−semiconductor boundary may have dominantly contributed. The intensities of the two electrodes became equal at a delay time of 50 ps, as shown in Figure 3c. The capacitor was fully discharged, and the two electrodes had the same voltage. Following a long delay time of τ = 625 ps, the cathodes were slightly brighter, as shown in Figure 3d. This indicated that the capacitor started to be recharged because the photoexcited carriers in the substrate were fully recombined. The lifetime of the photoexcited carriers in undoped GaAs at room temperature was less than 500 ps, which is consistent with previous reports.[33,34] The ultrafast change in the effective voltage applied to the cathodes was plotted as a function of delay time, τ = 0, as shown in Figure 3e. The voltage reduced rapidly at approximately τ = 0 ps and starts to recovers after τ = 500 ps. The data were fitted using a step function with a finite rise time $f(\tau) = y_0 + y_1/[1 + \exp(-4\tau/\delta)]$, where the rising time δ = 43 ps was the duration in which the signal changed from 12 to 88% between y_0 and y_1 (smallest and largest values). These results demonstrate the successful development of a SUEM with a temporal resolution of 43 ps (bandwidth >20 GHz). Notably, the temporal resolution δ was dominantly contributed by the duration of the electron pulse because the response time (RC time) of the bright state of the IDA was estimated as 21 ps (see, Supporting Information S9), which is smaller than the δ. This technique can be utilized to visualize the transient response of an electric potential at an arbitrary position on high-frequency electronic devices, which is difficult to achieve by using conventional oscilloscope measurements.

To comprehensively evaluate the duration of the electron pulses, we discuss the space charge effect. The duration and shape of an electron pulse can be altered by increasing the number of electrons per pulse. Figure 4a shows the time-resolved SE intensity on a cathode of photoexcited IDA with different powers of 4ω light: 40, 80, and 160 mW. The number of electrons in a pulse increased by increasing the power of 4ω such that the pulse duration of electrons was stretched by Coulombic repulsion between electrons in the same pulse. The electrons at the front end of a pulse were accelerated, and the back-end electrons were decelerated. Here, we assumed the temporal shape of the electron pulse as a rectangle function $f(\tau,T)$ with the duration of T, and the response function of the IDA as a step function $g(\tau,\Delta) = 1/(1 + \exp[-4\tau/\Delta])$ with finite rising time Δ. We used the convoluted function $h(\tau) = y_0 + y_1 \int_{-\infty}^{\infty} f(t,T)g(\tau - t,\Delta)dt$ as the fitting function (further details are given in the Supporting Information). The fitting results are shown as deep-colored curves in Figure 4a. The temporal waveforms of the experimental results were well reproduced, and the rectilinear shape at approximately τ = 0 became pronounced by increasing the power. The parameters of Δ and T are plotted in Figure 4b. The T had the minimum value of 42 ± 3.2 ps at lower power and increased to 143 ± 1.0 ps with the power of 160 mW (3.2×10^4 electrons/pulse) owing to the space charge effect. Notably, the response time of $\Delta \sim$ 18 ps did not change by changing the number of probe electrons. Here, 18 ps indicates the recombination of charges

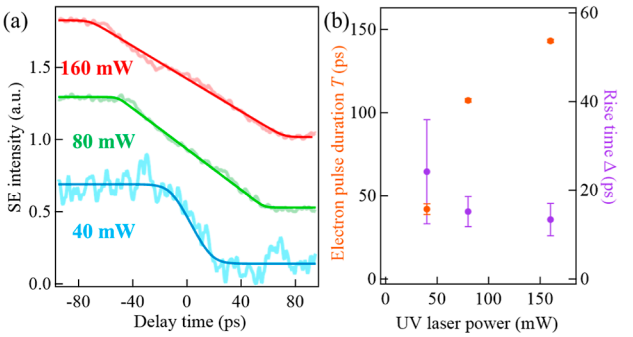

Figure 4. (a) Transient change in the cathode intensity of the IDA device with different 4ω powers changed by using a neutral density filter on a rotational mount. The value of 40 mW is the same as that used in the measurements in Figure 3; V_b = −20 V. The number of electrons per pulse was measured by the current on the sample holder to the ground. Light color curves are measured results, and deep color curves are fitted results (see the main text). (b) Duration of the electron pulses (orange, left axis) and the rise time of the sample (purple, right axis) derived by the fitting.

https://doi.org/10.1021/acsphotonics.3c01532
ACS Photonics 2024, 11, 2171−2175

close to the metal−semiconductor boundary. This analysis deconvoluted the pulse durations of the electron and carrier dynamics. Notably, the correlation between the Δ and T becomes large in the lowest power. Therefore, the temporal resolution should be determined by δ = 43 ps, as shown in Figure 3i.

CONCLUSIONS

We performed SUEM to obtain direct images of the electric potentials of the operand electric devices. We successfully visualized the photoconductive switching of IDAs on a GaAs substrate with a temporal resolution of 43 ps. The carrier dynamics of the sample and the space charge effect were discussed by assuming a rectangular waveform for electron pulses. The waveform of the SE current exhibited ultrafast electronic dynamics at the boundaries, carrier lifetimes, and electric circuit responses. The temporal resolution can be improved to reduce the influence of the space charge effect. This technique is expected to provide a direct and comprehensive understanding of the operational dynamics of high-frequency electronic devices.

ASSOCIATED CONTENT

Supporting Information

The Supporting Information is available free of charge at https://pubs.acs.org/doi/10.1021/acsphotonics.3c01532.

Time-resolved snapshots (MP4)

Additional experimental details, materials, and methods, including photographs of experimental setup (PDF)

AUTHOR INFORMATION

Corresponding Authors

Yusuke Arashida − *Institute of Pure and Applied Science, University of Tsukuba, Tsukuba 305-8573, Japan;* orcid.org/0000-0001-6366-3934; Email: arashida.yusuke.kb@u.tsukuba.ac.jp

Samuel Jeong − *Institute of Pure and Applied Science, University of Tsukuba, Tsukuba 305-8573, Japan;* orcid.org/0000-0003-2231-7271; Email: jeong.samuel.fp@u.tsukuba.ac.jp

Jun-ichi Fujita − *Institute of Pure and Applied Science, University of Tsukuba, Tsukuba 305-8573, Japan;* Email: fujita.junichi.fu@u.tsukuba.ac.jp

Authors

Kouhei Kawasaki − *Institute of Pure and Applied Science, University of Tsukuba, Tsukuba 305-8573, Japan*

Yuga Emoto − *Institute of Pure and Applied Science, University of Tsukuba, Tsukuba 305-8573, Japan*

Godai Noyama − *Institute of Pure and Applied Science, University of Tsukuba, Tsukuba 305-8573, Japan*

Masaki Hada − *Institute of Pure and Applied Science, University of Tsukuba, Tsukuba 305-8573, Japan; Tsukuba Research Center for Energy Materials Science (TREMS), University of Tsukuba, Tsukuba 305-8573, Japan;* orcid.org/0000-0001-8148-0971

Yoshiya Kishibe − *Institute of Pure and Applied Science, University of Tsukuba, Tsukuba 305-8573, Japan*

Hidemi Shigekawa − *Institute of Pure and Applied Science, University of Tsukuba, Tsukuba 305-8573, Japan;* orcid.org/0000-0001-9550-5148

Keishi Akada − *Institute of Pure and Applied Science, University of Tsukuba, Tsukuba 305-8573, Japan*

Shoji Yoshida − *Institute of Pure and Applied Science, University of Tsukuba, Tsukuba 305-8573, Japan*

Complete contact information is available at: https://pubs.acs.org/10.1021/acsphotonics.3c01532

Author Contributions

Y.A., S.J., K.K., and Y.E. developed the system and collected the data. Y.K., H.S., K.A., and S.Y. provided technical advice. Y.A., G.N., and M.H. provided the numerical calculations. J.F. organized and supervised the project. Y.A., S.J., and J.F. edited the paper.

Funding

Y.A., S.J., H.S., K.A., S.Y, and J.F were supported by the Innovative Science and Technology Initiative for Security, ATLA, Japan (JPJ004596). This work was partly supported by the grant-in-aid for JSPS KAKENHI (19H00847 and 22H00289).

Notes

The authors declare no competing financial interest.

REFERENCES

(1) Wang, Q. H.; Kalantar-zadeh, K.; Kis, A.; Coleman, J. N.; Strano, M. S. Electronics and optoelectronics of two-dimensional transition metal dichalcogenides. *Nat. Nanotechnol.* **2012**, *7*, 699−712.

(2) Choi, W. K.; Liew, T. H.; Dawood, M. K.; Smith, H. I.; Thompson, C. V.; Hong, M. Synthesis of silicon nanowires and nanofin arrays using interference lithography and catalytic etching. *Nano Lett.* **2008**, *8*, 3799−3802.

(3) Mourou, G. A.; Meyer, K. E. Subpicosecond electro-optic sampling using coplanar strip transmission lines. *Appl. Phys. Lett.* **1984**, *45*, 492−494.

(4) Pospischil, A.; Humer, M.; Furchi, M. M.; Bachmann, D.; Guider, R.; Fromherz, T.; Mueller, T. CMOS-compatible graphene photodetector covering all optical communication bands. *Nat. Photonics* **2013**, *7*, 892−896.

(5) Kan, T.; Isozaki, A.; Kanda, N.; Nemoto, N.; Konishi, K.; Takahashi, H.; Kuwata-Gonokami, M.; Matsumoto, K.; Shimoyama, I. Enantiomeric switching of chiral metamaterial for terahertz polarization modulation employing vertically deformable MEMS spirals. *Nat. Commun.* **2015**, *6*, 8422.

(6) Gramotnev, D. K.; Bozhevolnyi, S. I. Plasmonics beyond the diffraction limit. *Nat. Photonics* **2010**, *4*, 83−91.

(7) Zworykin, V. K. The Scanning Electron Microscope. *Sci. Am.* **1942**, *167*, 111−113.

(8) Oatley, C. W. The Early History of the Scanning Electron Microscope. *Adv. Imaging Electron Phys.* **1982**, *53*, R1−R13.

(9) Yao, J. J. RF MEMS from a Device Perspective. *J. Manuf. Syst.* **2000**, *10*, R9−R38.

(10) Midolo, L.; Schliesser, A.; Fiore, A. Nano-Opto-Electro-mechanical Systems. *Nat. Nanotechnol.* **2018**, *13*, 11−18.

(11) Ong, C. B.; Ng, L. Y.; Mohammad, A. W. A review of ZnO nanoparticles as solar photocatalysts: Synthesis, mechanisms and applications. *Renew. Sustain. Energy Rev.* **2018**, *81*, 536−551.

(12) Valentine, J.; Zhang, S.; Zentgraf, T.; Ulin-Avila, E.; Genov, D. A.; Bartal, G.; Zhang, X. Three-Dimensional Optical Metamaterial with a Negative Refractive Index. *Nature* **2008**, *455*, 376−379.

(13) Gansel, J. K.; Thiel, M.; Rill, M. S.; Decker, M.; Bade, K.; Saile, V.; von Freymann, G.; Linden, S.; Wegener, M. Gold Helix Photonic Metamaterial as Broadband Circular Polarizer. *Science* **2009**, *325*, 1513−1515.

(14) Xiao, S.; Wang, T.; Liu, T.; Zhou, C.; Jiang, X.; Zhang, J. Active metamaterials and metadevices: a review. *J. Phys. D: Appl. Phys.* **2020**, *53*, 503002.

(15) Ren, Z.; Chang, Y.; Ma, Y.; Shih, K.; Dong, B.; Lee, C. Leveraging of MEMS Technologies for Optical Metamaterials Applications. *Adv. Opt. Mater.* **2020**, *8*, 1900653.
(16) Mohammed, O. F.; Yang, D. S.; Pal, S. K.; Zewail, A. H. 4D Scanning Ultrafast Electron Microscopy: Visualization of Materials Surface Dynamics. *J. Am. Chem. Soc.* **2011**, *133*, 7708−7711.
(17) Cho, J.; Hwang, T. Y.; Zewail, A. H. Visualization of carrier dynamics in p(n)-type GaAs by scanning ultrafast electron microscopy. *Proc. Natl. Acad. Sci. U.S.A.* **2014**, *111*, 2094−2099.
(18) Sun, J.; Melnikov, V. A.; Khan, J. I.; Mohammed, O. F. Real-Space Imaging of Carrier Dynamics of Materials Surfaces by Second-Generation Four-Dimensional Scanning Ultrafast Electron Microscopy. *J. Phys. Chem. Lett.* **2015**, *6*, 3884−3890.
(19) Liao, B.; Najafi, E.; Li, H.; Minnich, A. J.; Zewail, A. H. Photo-excited hot carrier dynamics in hydrogenated amorphous silicon imaged by 4D electron microscopy. *Nat. Nanotechnol.* **2017**, *12*, 871−876.
(20) Bose, R.; Adhikari, A.; Burlakov, V. M.; Liu, G.; Haque, M. A.; Priante, D.; Hedhili, M. N.; Wehbe, N.; Zhao, C.; Yang, H.; Ng, T. K.; Goriely, A.; Bakr, O. M.; Wu, T.; Ooi, B. S.; Mohammed, O. F. Imaging Localized Energy States in Silicon-Doped InGaN Nanowires Using 4D Electron Microscopy. *ACS Energy Lett.* **2018**, *3*, 476−481.
(21) Zani, M.; Sala, V.; Irde, G.; Pietralunga, S. M.; Manzoni, C.; Cerullo, G.; Lanzani, G.; Tagliaferri, A. Charge dynamics in aluminum oxide thin film studied by ultrafast scanning electron microscopy. *Ultramicroscopy* **2018**, *187*, 93−97.
(22) Najafi, E.; Jafari, A. Ultrafast imaging of surface-exclusive carrier dynamics in silicon. *J. Appl. Phys.* **2019**, *125*, 185303.
(23) Garming, M. W. H.; Bolhuis, M.; Conesa-Boj, S.; Kruit, P.; Hoogenboom, J. P. Lock-In Ultrafast Electron Microscopy Simultaneously Visualizes Carrier Recombination and Interface-Mediated Trapping. *J. Phys. Chem. Lett.* **2020**, *11*, 8880−8886.
(24) Li, Y.; Choudhry, U.; Ranasinghe, J.; Ackerman, A.; Liao, B. Probing Surface Photovoltage Effect Using Photoassisted Secondary Electron Emission. *J. Phys. Chem. A* **2020**, *124*, 5246−5252.
(25) Wohltjen, H.; Dessy, R. Surface acoustic wave probe for chemical analysis. I. Introduction and instrument description. *Anal. Chem.* **1979**, *51*, 1458−1464.
(26) Wang, J.; Ota, S.; Edlbauer, H.; Jadot, B.; Mortemousque, P. A.; Richard, A.; Okazaki, Y.; Nakamura, S.; Ludwig, A.; Wieck, A. D.; Urdampilleta, M.; Meunier, T.; Kodera, T.; Kaneko, N.; Takada, S.; Bäuerle, C. Generation of a Single-Cycle Acoustic Pulse: A Scalable Solution for Transport in Single-Electron Circuits. *Phys. Rev. X.* **2022**, *12*, 031035.
(27) Richard, S. W.; Gerard, H. M.; Collins, J. H.; Reeder, M.; Shaw, H. J. Design with of Surface Interdigital Wave Delay Lines. *IEEE, Trans. Microw. Theory Technol.* **1969**, *17*, 865−873.
(28) Burford, N. M.; El-Shenawee, M. O. Review of terahertz photoconductive antenna technology. *Opt. Eng.* **2017**, *56*, 010901.
(29) Yardimci, N. T.; Jarrahi, M. Nanostructure-Enhanced Photoconductive Terahertz Emission and Detection. *Small* **2018**, *14*, 1802437.
(30) Matthäus, G.; Nolte, S.; Hohmuth, R.; Voitsch, M.; Richter, W.; Pradarutti, B.; Riehemann, S.; Notni, G.; Tünnermann, A. microlens coupled interdigital photoconductive switch. *Appl. Phys. Lett.* **2008**, *93*, 091110.
(31) Horsley, A.; Appel, P.; Wolters, J.; Achard, J.; Tallaire, A.; Maletinsky, P.; Treutlein, P. Microwave Device Characterization Using a Widefield Diamond Microscope. *Phys. Rev. Appl.* **2018**, *10*, 044039.
(32) Yang, Y.; Gao, A.; Lu, R.; Gong, S. 5-GHz Lithium Niobate MEMS Resonators with High FoM of 153. *2017 IEEE 30th International Conference on Micro Electro Mechanical Systems (MEMS)*; IEEE, 2017; pp 942−945.
(33) Prabhu, S. S.; Ralph, S. E.; Melloch, M. R.; Harmon, E. S. Carrier dynamics of low-temperature-grown GaAs observed via THz spectroscopy. *Appl. Phys. Lett.* **1997**, *70*, 2419−2421.
(34) Ahrenkiel, R. K.; Al-Jassim, M. M.; Dunlavy, D.; Jones, K.; Vernon, S.; Tobin, S.; Haven, V. Minority carrier lifetime of GaAs on silicon. *J. Electrochem. Soc.* **1988**, *137*, 996−1000.

https://doi.org/10.1021/acsphotonics.3c01532
ACS Photonics 2024, 11, 2171−2175